Efficacy of Systemically Administered Mutant Vesicular Stomatitis Virus (VSVΔ51) Combined with Radiation for Nasopharyngeal Carcinoma

Nehad M. Alajez,[1,2] Joseph D. Mocanu,[1,2] Wei Shi,[1,2] Marie C. Chia,[1,2] Caroline J. Breitbach,[7,8] Angela B.Y. Hui,[1,2] Shane Knowles,[8] John C. Bell,[7,8] Pierre Busson,[9] Kenzo Takada,[10] Kwok-Wai Lo,[11] Brian O'Sullivan,[3,5] Pat Gullane,[4,6] and Fei-Fei Liu[1,2,3,4,5]

Abstract

Purpose: Nasopharyngeal carcinoma (NPC) is a malignancy of the head and neck region that is associated with EBV latency. Curative treatments for NPC achieve modest survival rates, underscoring a need to develop novel therapies. We evaluated the therapeutic potential of a mutant vesicular stomatitis virus (VSVΔ51) as single treatment modality or in combination with ionizing radiation (RT) in NPC.

Experimental Design: MTS assay was used to assess cell viability *in vitro*; apoptosis was measured using propidium iodide staining and caspase activation. *In vivo* experiments were conducted using tumor-bearing nude mice with or without local RT (4 Gy). Apoptosis was assessed in excised tumor sections with terminal deoxynucleotidyl transferase–mediated dUTP nick end labeling staining.

Results: Our data showed that NPC cells are exquisitely sensitive to VSVΔ51 oncolysis, which correlated with the presence of EBV. Efficacy of VSVΔ51 against NPC cells was further augmented when combined with RT. A single systemic injection of VSVΔ51 achieved 50% survival in treated mice, which increased to 83% when combined with local tumor RT. In addition to induction of apoptosis, an antiangiogenic effect of VSVΔ51 was observed *in vivo*, suggesting a novel tumoricidal mechanism for VSVΔ51. This virus also prevented growth of NPC sphere-forming cells *in vitro*, showing potential utility in targeting NPC-initiating cells.

Conclusions: Our data represent the first report showing that EBV-positive NPC cells are exquisitely sensitive to VSVΔ51 oncolysis and documenting the successful utilization of this combinatorial regimen as a novel curative therapeutic strategy for NPC.

Head and neck cancer is the fifth most common malignancy worldwide, affecting ~946,745 individuals annually (1). Almost one-fifth of the total global cancer burden is associated with bacterial or viral infections (2); among these, nasopharyngeal carcinoma (NPC) represents a unique head and neck cancer, which is almost always associated with the EBV (3). The EBV episome is maintained in a latent phase within NPC cells, expressing a restricted set of genes including EBNA1, LMP1, LMP2A, and LMP2B (4), along with the presence of EBV-encoded RNA (5). Standard therapy for NPC patients comprise ionizing radiation (RT) only for early disease, with the addition of chemotherapy for patients with advanced disease. Using conformal or intensity-modulated RT, excellent local control can be attained; however, 43% of patients will still develop distant metastases within 2 years (6). This modest clinical outcome underscores the necessity to develop novel therapies for NPC, which has been the research focus of our group for the past several years (7–9). Our previous treatment approaches (viral and molecular) showed promising results yet were unable to achieve complete eradication of established nasopharyngeal tumors.

Authors' Affiliations: [1]Division of Applied Molecular Oncology, Ontario Cancer Institute; Departments of [2]Medical Biophysics, [3]Radiation Oncology, and [4]Otolaryngology, University of Toronto; Departments of [5]Radiation Oncology and [6]Surgical Oncology, University Health Network, Toronto, Ontario, Canada; [7]Centre for Cancer Therapeutics, Ottawa Health Research Institute; [8]Department of Biochemistry, Microbiology and Immunology, University of Ottawa, Ottawa, Ontario, Canada; [9]Institut Gustave Roussy, Villejuif, France; [10]Department of Tumor Virology, Institute for Genetic Medicine, Hokkaido University, Sapporo, Japan; [11]Department of Anatomical and Cellular Pathology, The Chinese University of Hong Kong, Hong Kong, People's Republic of China

Received 9/7/07; revised 3/10/08; accepted 3/31/08.

Grant support: Canadian Institutes of Health Research and Elia Chair in Head and Neck Cancer Research.

The costs of publication of this article were defrayed in part by the payment of page charges. This article must therefore be hereby marked *advertisement* in accordance with 18 U.S.C. Section 1734 solely to indicate this fact.

Note: Supplementary data for this article are available at Clinical Cancer Research Online (http://clincancerres.aacrjournals.org/).

Requests for reprints: Fei-Fei Liu, Department of Radiation Oncology, Princess Margaret Hospital/Ontario Cancer Institute, 610 University Avenue, Toronto, Ontario, Canada M5G 2M9. Phone: 416-946-2123; Fax: 416-946-4586; E-mail: Fei-Fei.Liu@rmp.uhn.on.ca.

doi:10.1158/1078-0432.CCR-07-4134

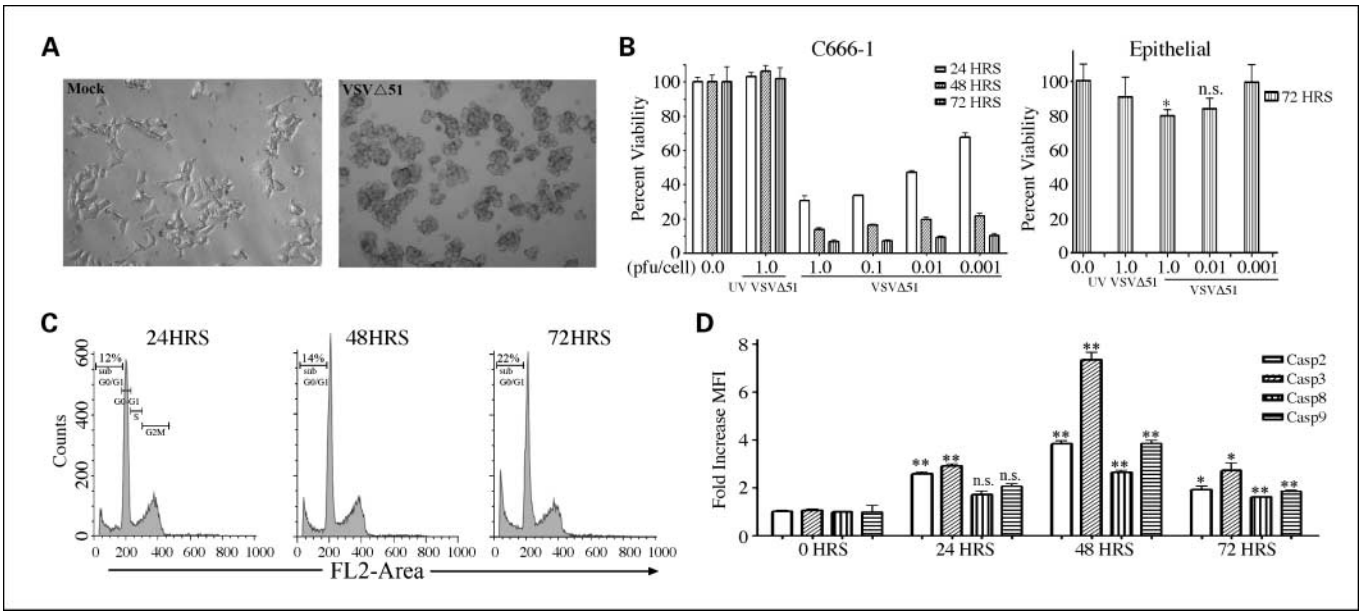

Fig. 1. VSVΔ51 infects C666-1 cells and induces apoptosis. *A,* C666-1 cells were infected with VSVΔ51-GFP (1 pfu/cell); 48 h later, mock (*left*) or VSV-infected (*right*) cells were visualized under light microscopy. *B,* MTS assay for C666-1 cells (*left*) or normal human oral epithelial cells (*right*) viability at the indicated time points following VSVΔ51 infection. Mean ± SD from experiments conducted in triplicate. *C,* representative experiment of propidium iodide staining of C666-1 cells infected with VSVΔ51-GFP (1 pfu/cell) at 24, 48, and 72 h. *D,* fold increase of caspase activation in C666-1 cells following VSVΔ51-GFP infection (1 pfu/cell) at 24, 48, and 72 h compared with mock-infected cells for each time point. Mean ± SE from at least two independent experiments conducted in triplicate. *, $P < 0.05$; **, $P < 0.005$.

Recently, mutant VSV strains (AV1 and AV2), which lack the ability to shut down the host innate immunity, have been described (10). Toxicity experiments showed that the AV1 mutant was ~80-fold less toxic than the wild-type VSV while maintaining similar antitumor efficacy, showing a therapeutic window for these mutant VSV strains. In the current report, the therapeutic potential of using a mutant (VSVΔ51) virus for EBV-positive NPC was investigated either alone or in combination with RT. When VSVΔ51 was combined with RT, an additive antitumor effect was observed both *in vitro* and *in vivo*. In addition, an antiangiogenic effect of VSVΔ51 was also apparent, suggesting a novel tumoricidal mechanism for VSVΔ51. These results show a novel therapeutic approach for NPC, by combining VSVΔ51 with RT, which appears to be particularly effective in EBV-positive disease.

Materials and Methods

Cell lines and reagents. C666-1, CNE-1, CNE1-EBV, HONE1, and HK-1 NPC lines were described previously (11–13). C15 and C17 nasopharyngeal xenograft tumors were maintained *in vivo* (14). Human oral epithelial cells were obtained from Celprogen and were cultured according to company recommendations. Other cells were maintained in RPMI 1640 supplemented with 10% fetal bovine serum, 100 mg/L penicillin, and 100 mg/L streptomycin (RPMI-10) at 37°C, 5% CO_2. The VSVΔ51-green fluorescent protein (GFP) virus has been described previously (10).

Cell infection. Twenty-thousand cells were seeded in 100 μL RPMI-10 in a 96-well plate. Twenty-four hours later, the medium was removed, and VSVΔ51-GFP [10-0.0001 plaque-forming units (pfu)/cell] was added in 20 μL α-MEM, with the plates maintained at 37°C for 60 min to allow virus attachment before the addition of 80 μL normal growth medium (RPMI-10). UV inactivation was done by exposing the virus for 30 min at 10 cm distance under UV light.

Cell viability and measurement of apoptosis. Cell viability was assessed using the MTS assay according to the manufacturer's recommended protocol (Promega). To measure the fraction of cells in the sub-G_0-G_1 phase of the cell cycle, C666-1 cells were infected with VSVΔ51-GFP at 1 pfu/cell, and at indicated time points, cells were harvested and fixed in 70% ethanol for 1 h on ice. Cells were washed once before resuspending in 500 μL fluorescence-activated cell sorting buffer (PBS/0.5% bovine serum albumin) supplemented with 40 μg/mL RNase A (Sigma) and 50 μg/mL propidium iodide. Cells were incubated at room temperature for 30 min in the dark before being analyzed in BD FACSCalibur using FL-2A and FL-2W channels. Cell debris was gated out before the analysis. CaspGlow kit (Biovision) was used to measure caspase activity in virally infected C666-1 cells.

NPC sphere culture. C15 and C17 NPC xenografts were propagated in severe combined immunodeficient mice. The tumor was excised on reaching 1 cm in diameter, cut into small pieces, minced with a scalpel, and then digested with 200 units/mL collagenase type I (Worthington Biochemical) in HBSS. The mixture was incubated for 1.5 h at 37°C, 5% CO_2 followed by repeated pipetting using a 10 mL pipette every 15 to 20 min. Cells were then filtered through a 40 μm cell strainer (BD Biosciences). Cells infected with VSVΔ51 or with UV-inactivated virus were seeded in T75 flask at 1×10^6 per 20 mL RPMI-10 and then incubated at 37°C, 5% CO_2. The number of subsequent NPC spheres (NPCS) was counted on day 21.

Animal experiments. CD-1 nude male mice (5-6 weeks old) were purchased from Charles River Laboratories; all experiments were conducted in accordance with the guidelines of the Animal Care Committee, University Health Network. For tumor formation assays, 1×10^6 C666-1 cells were infected at 5 pfu/cell in α-MEM for 1 h, spun down, and then resuspended in 100 μL PBS before s.c. implantation in CD-1 nude mice. Tumor volume was measured using the formula: $V = LWW / 2$, where L and W represent tumor length and width, respectively. For therapeutic experiments, 3×10^6 C666-1 cells were injected either s.c. on the upper hind flank or i.m. into the left leg. When tumor volume reached 100 mm^3 (for the sc model) or when tumor plus leg diameter reached 8.5 to 9.5 mm (for the i.m. model), treatment was initiated. Mice were treated as indicated by injecting the appropriate dose of virus in 100 μL PBS i.v. via tail vein. For local radiation treatment, animals were immobilized in a lucite box with the

tumor-bearing leg exposed to 100 kV at a dose rate of 10 Gy/min (Gemini Vertical X-ray Beam, Picker Industrial).

Microdistribution studies. CD-1 nude mice bearing C666-1 tumors were injected i.v. with 5×10^8 VSVΔ51-GFP in 100 μL PBS. At 24, 96, or 144 h postinjection, Hoechst 33342 (600 μg in 100 μL PBS) was injected i.v. for visualization of active vasculature (15); the mice were sacrificed 1 min later. Tumors were immediately excised, frozen in OCT compound (Bayer) and then stored at -80°C. Serial sections (5 μm thickness) were cut through each tumor at three levels, 500 μm apart.

The slides were scanned using a fluorescence microscope to visualize GFP expression and Hoechst 33342 perfusion and were then stained with rat anti-mouse CD31 antibody (BD PharMingen) at 1:500 dilution followed by secondary incubation with anti-rat biotinylated antibody and tertiary incubation with FITC-conjugated streptavidin to fluorescently visualize total tumor vasculature. The slides were then stained with terminal deoxynucleotidyl transferase–mediated dUTP nick end labeling to assess for apoptosis or necrosis. All staining and cryosectioning procedures were done by the Pathology Research Services, University Health Network.

Microscopy. Unstained and FITC anti-CD31-stained slides were imaged at ×10 magnification using an Olympus BX50 tiling fluorescence stereomicroscope (FITC/GFP: λ_{ex} = 482 nm, λ_{em} = 535 nm, 500 ms exposure; Hoechst 33342: λ_{ex} = 360 nm, λ_{em} = 460 nm, 100 ms exposure). Images were captured using ImagePro 5.1 (Media Cybernetics). Terminal deoxynucleotidyl transferase–mediated dUTP nick end labeling slides were scanned at ×20 magnification using an Aperio ScanScope CS automated tiling bright-field microscope (Aperio). Fluorescence microscopy images were imported into ImageJ (NIH),[12] false colored, and merged into a composite image, where the red, green, and blue channels corresponded to Hoechst 33342 (active vasculature), GFP (VSV infection), and FITC anti-CD31 (total vasculature), respectively. For the quantification of VSV replication and tumor vascular functionality, four square regions (~100 × 100 μm) were taken per slide for each time point, and pixel intensity values for all three channels (green, red, and blue) were calculated as described before (16).

Statistical analysis. Statistical analyses and graphing were done using Microsoft Excel 2003 and Graphpad Prism 4.0 software.

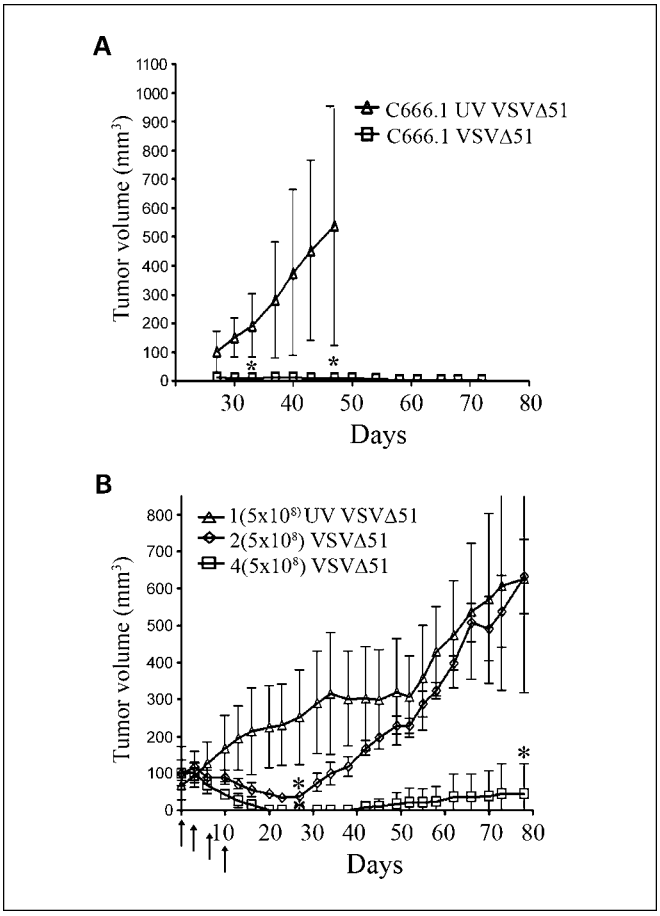

Fig. 2. VSVΔ51 is effective against NPC *in vivo*. *A,* C666-1 cells were infected with UV-inactivated virus or with VSVΔ51 (5 pfu/cell) before implanting into CD1 nude mice. Each group comprised three mice. *B,* C666-1-bearing CD1 nude mice were treated i.v. with two injections (days 0 and 3) or four injections (days 0, 3, 7, and 10) of 5×10^8 VSVΔ51. Control mice received 5×10^8 UV-VSVΔ51 on day 0, and tumor volume was measured over time. Mean ± SD (n = 3 mice in each group). *, $P < 0.05$. *Arrow,* day of virus injections.

Results

***NPC cells are sensitive to VSVΔ51 infection* in vitro.** To evaluate if NPC cells are sensitive to VSVΔ51 infection, EBV-positive NPC C666-1 cells were infected with VSVΔ51-GFP and then examined morphologically. Figure 1A (*left*) shows the appearance of normal C666-1 cells; in contrast, VSVΔ51-infected cells were rounded and detached from the plate (Fig. 1A, *right*), consistent with the appearance of virally infected cells (17). VSVΔ51 was then examined as a single agent, showing significant toxicity in C666-1 cells in a dose- and time-dependent manner (Fig. 1B). By 72 h, even at 0.001 pfu/cell, 89.6% cytotoxicity was shown (Fig. 1B, *left*). In contrast, VSVΔ51 had no significant toxicity against normal human oral epithelial cells at 0.01 pfu/cell (Fig. 1B, *right*). Similarly, the virus exhibited no significant toxicity against the GM05757 normal human fibroblast line (data not shown).

VSVΔ51-GFP kills NPC cells by disrupting the cell membrane and inducing apoptosis. To elucidate the mode of cell death of NPC cells following VSVΔ51 infection, C666-1 cells were infected with VSVΔ51-GFP and at 24, 48, and 72 h postinfection and were stained with propidium iodide to assess membrane integrity. A time-dependent increase in the population of cells with damaged cell membranes was observed, reaching 45% at 72 h postinfection (data not shown). To assess if VSVΔ51 induced apoptosis, cell cycle analysis was done on VSVΔ51-infected C666-1 cells. Again, a time-dependent increase in the sub-G_0-G_1 population was observed, reaching 22% at 72 h postinfection (Fig. 1C). This increase in apoptosis was associated with activation of caspase-2, caspase-3, caspase-8, and caspase-9 (Fig. 1D), with maximal activation observed for the effector caspase-3 (7.3-fold) at 48 h postinfection.

Systemic administration of VSVΔ51 is effective against established nasopharyngeal xenograft tumors. To evaluate whether VSVΔ51 infection can prevent tumor formation *in vivo*, C666-1 cells were infected with VSVΔ51 at 5 pfu/cell before s.c. implantation into CD-1 nude mice. VSVΔ51-infected C666-1 cells failed to form tumors when monitored for >70 days, whereas cells treated with UV-inactivated VSVΔ51 formed tumors as early as 20 days postimplantation (Fig. 2A).

VSVΔ51 was then administered systemically to evaluate its therapeutic potential in mice bearing C666-1 tumors. Two injections of 5×10^8 VSVΔ51-GFP significantly reduced tumor growth compared with mice that received UV-inactivated virus (Fig. 2B). Four injections of VSVΔ51-GFP reduced tumor size below the detection limit as early as 25 days post-treatment;

[12] http://rsb.info.nih.gov/ij/

however, all tumors in this group eventually recurred. Treating tumor-bearing mice with six injections of 5×10^8 UV-inactivated virus had no significant effect on tumor growth (data not shown).

***RT in combination with VSVΔ51 is effective against NPC* in vitro.** Given the data in Figs. 1 and 2, RT was then added to evaluate efficacy of this combined approach. Surprisingly, RT-treated cells were less permissive to virus replication when compared with nonirradiated cells at 24 h post-RT *in vitro* (Supplementary Fig. S1A). This was transient, however; at 48 h, RT plus VSVΔ51-treated cells produced a similar viral titer compared with nonirradiated cells. Lower viral titer was again observed at 72 h likely attributable to the significant cytotoxicity with the combination treatment. RT plus VSVΔ51 killed >99.0% of C666-1 cells compared with 89.0% killing for the VSVΔ51 alone group on day 6 post-treatment (P = 0.005; Fig. 3A). Cell cycle analysis showed a slight increase in the percentage of apoptotic cells (sub-G_0-G_1) in the RT plus VSVΔ51 (30.6%) group compared with VSVΔ51 only (28.0%) at 72 h (Supplementary Fig. S1B). As expected, RT alone induced G_2-M arrest, which was significantly reduced when RT-treated cells were infected with VSVΔ51.

Efficacy of RT combined with VSVΔ51 on established nasopharyngeal xenograft tumors. To determine whether combining RT with VSVΔ51 was effective against established xenograft tumors, C666-1 tumors were generated and then randomized to six treatment groups. RT (4 Gy) alone caused significant reduction in tumor growth, which was less effective than single i.v. injection of VSVΔ51 (5×10^8 pfu; Fig. 3B). Three different schedules of RT plus VSVΔ51 were evaluated: simultaneously or 48 h apart, with either RT preceding VSVΔ51, or vice versa. The most effective combination was the simultaneous administration of RT with VSVΔ51, achieving almost complete tumor eradication, followed for 42 days. With longer follow-up time, and plotted as a function of survival, these data showed significant survival advantage for the group of mice treated with the simultaneous administration of RT plus VSVΔ51 (P = 0.0005), with 83% (5 of 6) mice surviving beyond 100 days (Fig. 3C).

No evidence of* in vivo *selection of VSV-resistant NPC cells following systemic administration of VSVΔ51. It has always been unclear whether tumors that regrow have acquired *in vivo* resistance to VSVΔ51 or if they have never been exposed to the virus. This issue was addressed by isolating tumor recurrences,

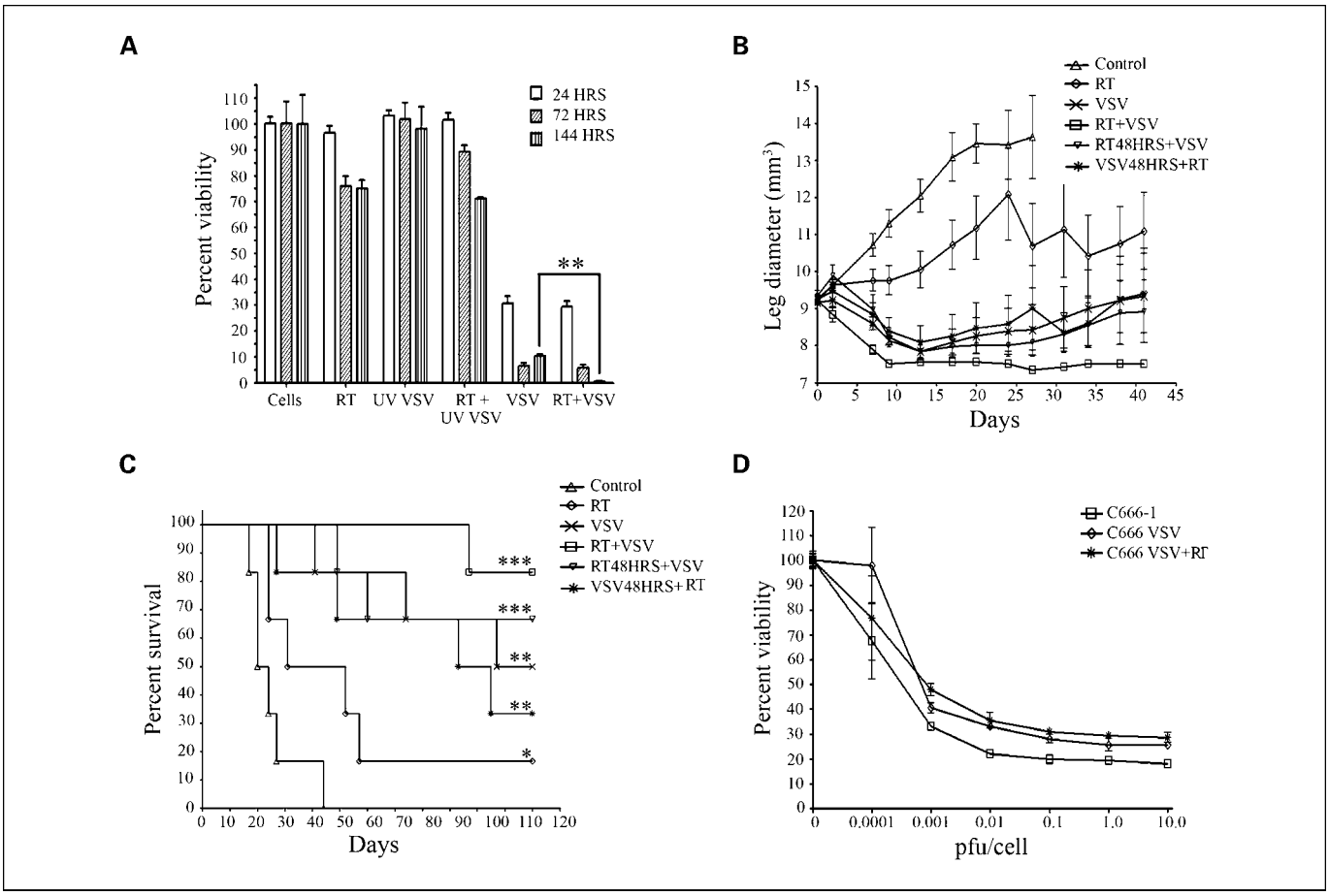

Fig. 3. VSVΔ51 in combination with RT is effective against NPC *in vitro* and *in vivo*. *A,* viability of C666-1 was measured using the MTS assay following VSVΔ51 (1 pfu/cell) or RT (6 Gy) plus VSVΔ51 at the indicated time points. Mean ± SE from at least two independent experiments conducted in triplicate. **, $P < 0.005$. *B,* C666-1 tumors were established i.m. in the left leg of CD1 nude mice to allow for local RT delivery. Mice were then randomized to six groups: (*a*) no treatment, (*b*) RT (4 Gy) alone, (*c*) VSV (5×10^8 pfu i.v.) alone, (*d*) RT plus VSV simultaneously, (*e*) RT preceding VSV by 48 h, and (*f*) VSV preceding RT by 48 h. Leg plus tumor diameter was monitored over time. Mean ± SE (n = 6 mice in each group). *C,* mice in *B* were monitored for survival for up to 120 days. All P values were calculated in comparison with the control group (*, $P < 0.05$; **, $P < 0.005$; ***, $P < 0.0005$). *D,* sensitivity of the parental C666-1 cells compared with C666-1 cells reestablished from tumor recurrences after VSVΔ51 administration or VSVΔ51 plus RT measured using the MTS assay. Mean ± SE (n = 6).

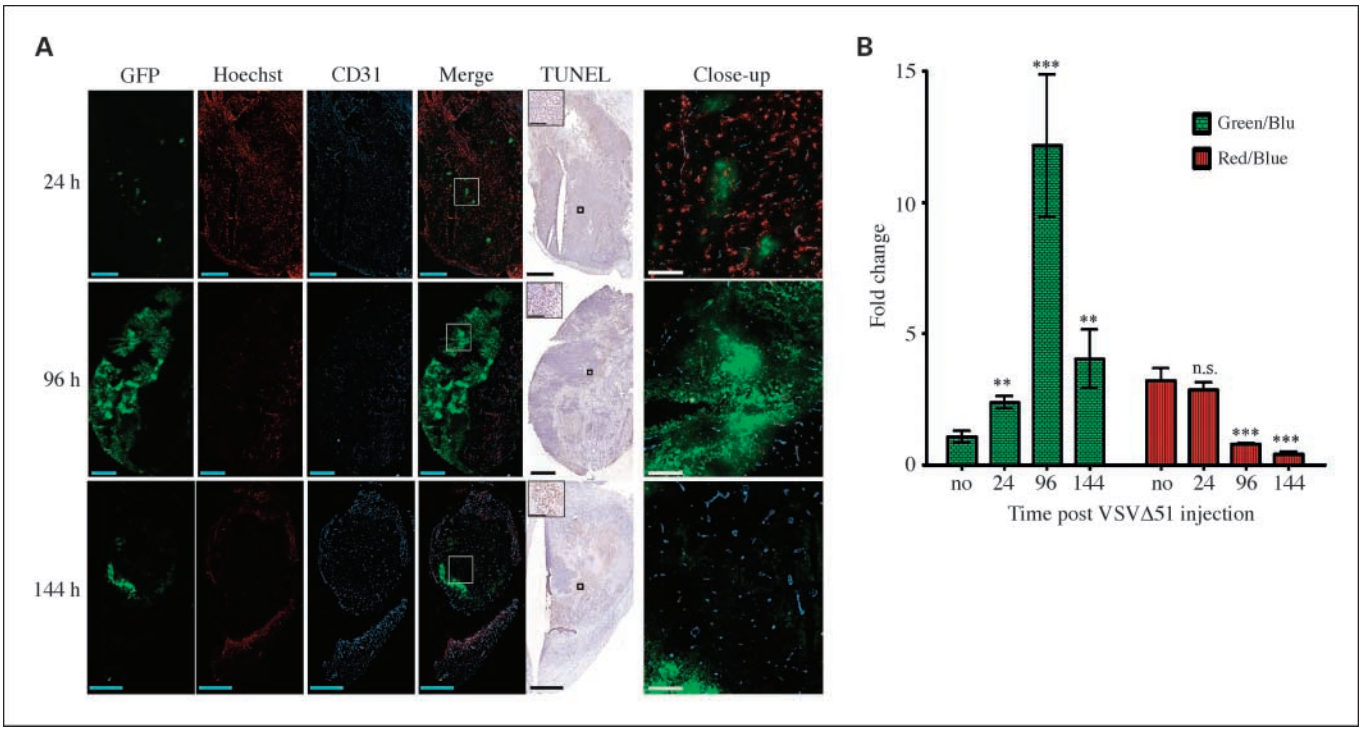

Fig. 4. Representative examples of VSVΔ51 tumor microdistribution in C666-1 xenograft tumors. *A,* viral distribution (GFP) was assessed at three time points (24, 96, and 144 h after infection) in relation to active vasculature (Hoechst, *red*), total vasculature (CD31, *blue*), and necrotic or apoptotic tissues (terminal deoxynucleotidyl transferase – mediated dUTP nick end labeling). The merged field consisted of superimposed VSV, Hoechst, and CD31 images; the close-up images (×100) are high-resolution representations of GFP distribution in relation to local blood vessels. Bars on the wide-field images (*cyan* and *black*), 1 mm. Bars on the terminal deoxynucleotidyl transferase – mediated dUTP nick end labeling close-up images, 125 μm. Bars on the close-up merged images (*white*), 200 μm. *B,* quantification of virus replication and tumor vascular functionality at the indicated time points was done by calculating the ratios of GFP/CD31 (*green/blue*) and Hoechst/CD31 (*red/blue*), respectively. Mean ± SD (n = 4). *no,* regions of no virus replication at 24 h. **, $P < 0.005$; ***, $P < 0.0005$.

following VSVΔ51 or RT plus VSVΔ51, and then reexposing to VSVΔ51 *in vitro*, which showed similar sensitivity compared with parental cells, indicating that tumors recurred likely due to inadequate exposure to VSVΔ51 *in vivo* (Fig. 3D).

VSVΔ51 replicates within C666-1 tumors and affects the tumor vasculature. The precise mechanism by which VSVΔ51 causes tumoricidal effects *in vivo* is still not fully elucidated. Hence, C666-1 tumor-bearing mice were treated with a single i.v. injection of VSVΔ51-GFP (5×10^8 pfu), and at 24, 96, and 144 h postinjection, the mice were injected i.v. with Hoechst 33342 (stains functional blood vessels) and sacrificed 1 min later. As early as 24 h postinjection, multiple foci of viral replication were observed (Fig. 4A, *green*), which colocalized with areas containing active blood vessels (*red*). CD31 staining was done to examine for total (functional and nonfunctional) blood vessels (*blue*). At 96 h postinjection, a marked increase in viral replication is clearly observed, accompanied by significant loss in staining for functional blood vessels (*red*) in regions of viral replication (Fig. 4A and B). Most of the tumor area still retained CD31 staining, suggesting that tumor vessel functionality (*red*) might have been destroyed, secondary to viral replication. At 144 h postinjection, there was a significant increase in terminal deoxynucleotidyl transferase – mediated dUTP nick end labeling staining (indicating apoptosis or necrosis), with minimal Hoechst 33342 uptake, indicating extensive tumor cell death.

***VSV kills NPCS-forming cells* in vitro.** C15 and C17 NPC xenografts can only be propagated in mice (14). When these nasopharyngeal tumors are cultured *in vitro*, the tumor-associated murine fibroblasts form a monolayer within a few days. After 3 to 4 weeks, NPC cells start to proliferate on top of the fibroblasts, forming a three-dimensional spheres (Fig. 5A), which we denoted as NPCS. Each NPCS likely originated from a single clonogen. To evaluate whether VSVΔ51 could prevent sphere formation *in vitro*, C15 and C17 xenografts were digested with collagenase, infected with VSVΔ51 or UV-inactivated virus, and seeded in RPMI-10. Three weeks later, the number of NPCS in each sample was counted. VSVΔ51 infection completely prevented NPCS formation *in vitro* for both NPC models (Fig. 5B); VSVΔ51 was also capable of destroying established C17 NPC within 72 h postinfection (Fig. 5C).

Discussion

We present here the first report documenting the successful utilization of the RNA oncolytic virus (VSVΔ51) in combination with RT for the treatment of NPC. This combinatorial strategy was extremely effective, causing complete regression of established nasopharyngeal xenograft tumors in >80% of treated mice, which appears superior to even our previous conditionally replicating adenovirus (18). Firstly, adenoviruses could only be administered using the intratumoral route because systemic administration result in significant liver expression and hepatotoxicity (19). In contrast, systemically administered VSVΔ51-GFP result in no GFP expression in either

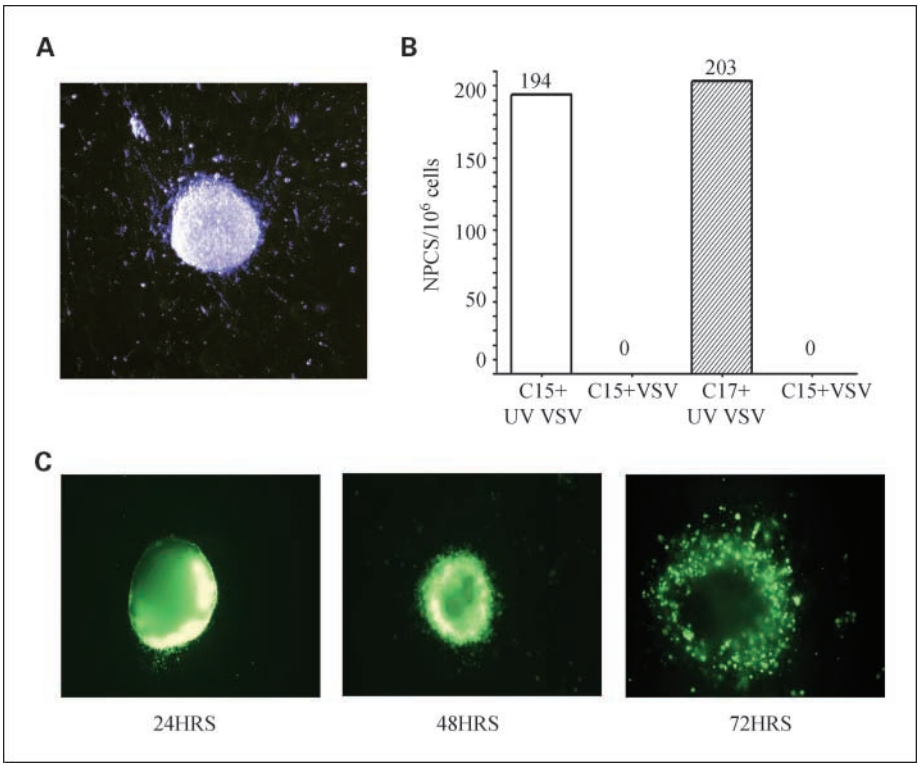

Fig. 5. VSVΔ51 is effective against NPCS *in vitro*. *A,* normal appearance of C17 NPCS in culture (day 21). *B,* number of C15 or C17 NPCS/10^6 cells forming after infection with either UV-inactivated virus (0.1 pfu/cell) or VSVΔ51-GFP (0.1 pfu/cell) on day 21 in culture. *C,* C17 NPCS infected with VSVΔ51-GFP (2×10^4 pfu) visualized using fluorescence microscopy at 24, 48, and 72 h postinfection.

the liver or the spleen of treated mice (data not shown), supporting the clinical utility of systemic administration of VSVΔ51 for NPC patients.

Secondly, a significant immune response is observed with even intratumoral adenoviral therapy, which again limits its tumoricidal efficacy. Certainly, repeated VSV would not be feasible in an immune-competent host, but with the combinatorial approach of local tumor RT with a single injection of VSVΔ51, significant tumor regression was achieved (Fig. 3B and C), thereby potentially bypassing the issue of VSV immunogenicity.

An important mode of cytotoxicity and tumoricidal effects of VSV appears to be apoptosis. In VSVΔ51-infected cells, activation of caspase-2, caspase-3, caspase-8, and caspase-9 were observed as early as 24 h postinfection, which is similar to that previously reported for murine fibroblasts following infection with another mutant (M51R-M) VSV (20). The interaction between RT and VSV is not well understood. RT can induce G_2-M arrest (21), but when VSVΔ51 infection follows RT, this G_2-M arrest was significantly reduced (Supplementary Fig. S1B), which might possibly relate to down-regulation of p53 function in VSVΔ51-infected cells (22, 23).

Yet another novel observation in this report relates to the exquisite sensitivity of NPC cells to VSVΔ51 as a function of EBV status (Supplementary Fig. S2). One possible explanation for this EBV-associated sensitivity to VSVΔ51 infection might relate to data generated from our own group showing induction of EBV lytic genes (*BZLF1* and *BRLF1*) when NPC cells are exposed to DNA damage via RT or chemotherapy (24). We have also observed an induction of these EBV lytic genes in NPC cells during VSVΔ51 infection (Supplementary Fig. S3), which might thereby enhance VSVΔ51 toxicity against NPC cells. The possible involvement of different EBV latent genes in this process remains to be investigated.

The third novel observation in this report relates to the apparent tumor vascular effects of VSVΔ51 infection *in vivo*. There is a clear time-dependent increase in viral replication following systemic administration of VSVΔ51 into NPC-bearing mice accompanied by tumor apoptosis or necrosis (Fig. 4A and B). Thus far, these data are consistent with other reports of apoptosis in glioblastoma xenograft tumors following intratumoral administration of wild-type VSV (25). Interestingly however, when we examined for active tumor vasculature (Hoechst 33342), there was an apparent time-dependent reduction in functional tumor blood vessels, suggesting that VSV could be targeting the tumor vasculature as another mechanism by which VSVΔ51 damages tumors. In fact, active viral replication was observed in tumor vascular endothelial cells as early as 24 h post-VSV injection (Supplementary Fig. S4); hence, these data, combined with the vascular functionality data (in Fig. 4), affirm a direct antivascular effect of this virus *in vivo*. Breitbach et al. have recently reported that tumor vessels are infiltrated by neutrophils following systemic administration of VSV, which would also impair vascular functionality (26). Concordantly, we also observed increased infiltration of nasopharyngeal tumors with neutrophils over time, suggesting additional tumoricidal effect of this virus against nasopharyngeal tumors *in vivo*.

There is increasing evidence of the existence of cancer stem cells (CSC) in human leukemias and solid tumors (27–29). The clonality of NPC and the presence of EBV genome in every NPC cell suggest that there might be a subpopulation of initiating or CSC in this malignancy. We have been able to culture NPC cells *in vitro*, derived originally from NPC

xenograft, to form three-dimensional colonies growing on top of a monolayer of murine fibroblasts. By definition, these NPCS have originated from a single NPC clonogen. Our data showed that VSVΔ51 is capable of infecting and destroying such NPCS *in vitro* and also preventing such spheres from forming, suggesting that VSVΔ51 could also target NPC CSC. It was shown recently that the interaction between vascular endothelial cells and CSC in brain tumors is crucial for the maintenance of "stemness" of such CSC (30). The use of antivascular agents was able to disrupt this interaction, thus ablating CSC from those xenografts. Because VSVΔ51 can also exert antivascular effects on NPC xenografts, this might therefore provide an alternate therapeutic option to inhibit NPC-initiating cells from self-renewal.

In conclusion, this is the first report of the exquisite efficacy of systemically administered VSVΔ51 in combination with RT for EBV-positive NPC. There are likely multiple mechanisms mediating this tumoricidal effect, including direct oncolysis, apoptosis, and antiangiogenesis. We propose that future NPC therapy should evaluate VSVΔ51 in the context of its ability to cure NPC, by eradicating the subpopulation of nasopharyngeal CSC, which could be responsible for recurrences and subsequent deaths of our NPC patients.

Disclosure of Potential Conflicts of Interest

J. Bell, financial interest in Jennerex Biotherapeutics. The other authors declare no potential conflicts of interest.

Acknowledgments

N.M. Alajez is a Canadian Institutes of Health Research Strategic Training Fellow in the Excellence in Radiation Research for the 21st Century (EIRR21) Program.

References

1. Parkin DM, Bray F, Ferlay J, Pisani P. Global cancer statistics, 2002. CA Cancer J Clin 2005;55:74–108.
2. Parkin DM. The global health burden of infection-associated cancers in the year 2002. Int J Cancer 2006;118:3030–44.
3. Raab-Traub N. Epstein-Barr virus in the pathogenesis of NPC. Semin Cancer Biol 2002;12:431–41.
4. Deacon EM, Pallesen G, Niedobitek G, et al. Epstein-Barr virus and Hodgkin's disease: transcriptional analysis of virus latency in the malignant cells. J Exp Med 1993;177:339–49.
5. Wu TC, Mann RB, Epstein JI, et al. Abundant expression of EBER1 small nuclear RNA in nasopharyngeal carcinoma. A morphologically distinctive target for detection of Epstein-Barr virus in formalin-fixed paraffin-embedded carcinoma specimens. Am J Pathol 1991;138:1461–9.
6. Lee N, Xia P, Quivey JM, et al. Intensity-modulated radiotherapy in the treatment of nasopharyngeal carcinoma: an update of the UCSF experience. Int J Radiat Oncol Biol Phys 2002;53:12–22.
7. Lax SA, Chia MC, Busson P, Klamut HJ, Liu FF. Adenovirus-p53 gene therapy in human nasopharyngeal carcinoma xenografts. Radiother Oncol 2001;61:309–12.
8. Li JH, Chia M, Shi W, et al. Tumor-targeted gene therapy for nasopharyngeal carcinoma. Cancer Res 2002;62:171–8.
9. Yip KW, Mocanu JD, Au PY, et al. Combination bcl-2 antisense and radiation therapy for nasopharyngeal cancer. Clin Cancer Res 2005;11:8131–44.
10. Stojdl DF, Lichty BD, ten Oever BR, et al. VSV strains with defects in their ability to shutdown innate immunity are potent systemic anti-cancer agents. Cancer Cell 2003;4:263–75.
11. Cheung ST, Huang DP, Hui AB, et al. Nasopharyngeal carcinoma cell line (C666-1) consistently harbouring Epstein-Barr virus. Int J Cancer 1999;83:121–6.
12. Huang DP, Ho JH, Poon YF, et al. Establishment of a cell line (NPC/HK1) from a differentiated squamous carcinoma of the nasopharynx. Int J Cancer 1980;26:127–32.
13. Iwakiri D, Sheen TS, Chen JY, Huang DP, Takada K. Epstein-Barr virus-encoded small RNA induces insulin-like growth factor 1 and supports growth of nasopharyngeal carcinoma-derived cell lines. Oncogene 2005;24:1767–73.
14. Busson P, Ganem G, Flores P, et al. Establishment and characterization of three transplantable EBV-containing nasopharyngeal carcinomas. Int J Cancer 1988;42:599–606.
15. Trotter MJ, Chaplin DJ, Durand RE, Olive PL. The use of fluorescent probes to identify regions of transient perfusion in murine tumors. Int J Radiat Oncol Biol Phys 1989;16:931–4.
16. Mocanu JD, Yip KW, Skliarenko J, et al. Imaging and modulating antisense microdistribution in solid human xenograft tumor models. Clin Cancer Res 2007;13:5935–41.
17. Spielhofer P, Bachi T, Fehr T, et al. Chimeric measles viruses with a foreign envelope. J Virol 1998;72:2150–9.
18. Chia MC, Shi W, Li JH, et al. A conditionally replicating adenovirus for nasopharyngeal carcinoma gene therapy. Mol Ther 2004;9:804–17.
19. Mocanu JD, Yip KW, Alajez NM, et al. Imaging the modulation of adenoviral kinetics and biodistribution for cancer gene therapy. Mol Ther 2007;15:921–9.
20. Gaddy DF, Lyles DS. Vesicular stomatitis viruses expressing wild-type or mutant M proteins activate apoptosis through distinct pathways. J Virol 2005;79:4170–9.
21. Abbott DW, Holt JT. Mitogen-activated protein kinase kinase 2 activation is essential for progression through the G_2-M checkpoint arrest in cells exposed to ionizing radiation. J Biol Chem 1999;274:2732–42.
22. Agarwal ML, Agarwal A, Taylor WR, Stark GR. p53 controls both the G_2-M and the G_1 cell cycle checkpoints and mediates reversible growth arrest in human fibroblasts. Proc Natl Acad Sci U S A 1995;92:8493–7.
23. Marques JT, Rebouillat D, Ramana CV, et al. Down-regulation of p53 by double-stranded RNA modulates the antiviral response. J Virol 2005;79:11105–14.
24. Chia MC, Leung A, Krushel T, et al. Nuclear factor-Y and Epstein Barr virus in nasopharyngeal cancer. Clin Cancer Res 2008;14:984–94.
25. Balachandran S, Porosnicu M, Barber GN. Oncolytic activity of vesicular stomatitis virus is effective against tumors exhibiting aberrant p53, Ras, or myc function and involves the induction of apoptosis. J Virol 2001;75:3474–9.
26. Breitbach CJ, Paterson JM, Lemay CG, et al. Targeted inflammation during oncolytic virus therapy severely compromises tumor blood flow. Mol Ther 2007;15:1686–93.
27. Lapidot T, Sirard C, Vormoor J, et al. A cell initiating human acute myeloid leukaemia after transplantation into SCID mice. Nature 1994;367:645–8.
28. Al-Hajj M, Wicha MS, Benito-Hernandez A, Morrison SJ, Clarke MF. Prospective identification of tumorigenic breast cancer cells. Proc Natl Acad Sci U S A 2003;100:3983–8.
29. Singh SK, Hawkins C, Clarke ID, et al. Identification of human brain tumour initiating cells. Nature 2004;432:396–401.
30. Calabrese C, Poppleton H, Kocak M, et al. A perivascular niche for brain tumor stem cells. Cancer Cell 2007;11:69–82.